Revista Internacional de Métodos Numéricos para Cálculo y Diseño en Ingeniería

Tech Science Press

https://doi.org/10.32604/rimni.2026.078765

ARTICLE

Deep Learning–Enhanced Fractional PID Control for Bidirectional DC–DC Converters in Electric Vehicles

Varaha Narasimha Raja Chilukoti[1], **Anand Gondesi**[2] **and Surender Reddy Salkuti**[3,*]

[1]Department of Electrical Engineering, Anil Neerukonda Institute of Technology and Sciences, Visakhapatnam, India
[2]Department of Electrical Engineering, Dr. Lankapalli Bullayya College of Engineering, Visakhapatnam, India
[3]Department of Global Railways, Woosong University, Daejeon, Republic of Korea

*Corresponding Author: Surender Reddy Salkuti. Email: surender@wsu.ac.kr

Received: 07 January 2026; Accepted: 12 February 2026; Published: 06 November 2026

ABSTRACT: This paper presents a deep learning–assisted fractional-order PID controller for a bidirectional DC–DC converter used in electric vehicle charging and discharging. The converter operates in buck mode during grid-to-vehicle operation and in boost mode during vehicle-to-grid operation. A deep neural network adaptively tunes the controller parameters to improve dynamic response under load and state-of-charge variation. The proposed DL-FOPID controller is evaluated against PID, FOPID, Type-2 fuzzy PID, and ANFIS controllers under identical simulation conditions. Performance is assessed in MATLAB/Simulink under step-load disturbances, mode transitions, load variation from 5 to 25 Ω, SOC variation from 100% to 20%, and multi-level charging and discharging between 10 to 30 A and −5 to −25 A. Results show up to 35% faster settling time, voltage deviation below 0.5 V, and lower overshoot and total harmonic distortion compared with the other controllers. The controller also demonstrates improved current tracking across all tested scenarios. Peak efficiency reaches 99% in simulation under optimal loading conditions. These results indicate that the DL-FOPID controller provides stable and robust performance for bidirectional DC–DC converter applications in electric vehicle power systems.

KEYWORDS: Deep learning; fractional-order PID; bidirectional DC–DC converter; electric vehicles; G2V; V2G; intelligent control

1 Introduction

As electric vehicles (EVs) have become more prevalent, there is an increasing need for efficient, reliable, and adaptable approaches to managing energy use [1]. Bidirectional DC–DC converters are necessary in these systems for vehicle-to-grid (V2G) discharging and grid-to-vehicle (G2V) charging [2]. Energy efficiency and reliability depend on maintaining a constant output voltage and current in the system through varying loads and battery status changes [3]. PID controllers have typically been used in power electronics control for their simplicity and proven effectiveness [4]. However, because of their fixed gains, PID devices cannot fully compensate for plant nonlinearities, parameter variations, and disturbances that are typical in the rapidly changing "vehicle to grid" environment [5]. FOPID devices have been suggested as a potential solution to some of these issues using fractional calculus from the PID framework [6]. Despite the better transient response and disturbance rejection offered by FOPID compared to classical PID, fast dynamic variations taking place within current EV powertrains may still be beyond their resolution capacity [7].

Copyright © 2027 The Authors. Published by Tech Science Press. This work is licensed under a Creative Commons Attribution 4.0 International License, which permits unrestricted use, distribution, and reproduction in any medium, provided the original work is properly cited.

Adaptive intelligent controllers such as the Type-2 Fuzzy PID and ANFIS-based FOPID have also been investigated to increase adaptability in uncertain and nonlinear conditions [8]. These techniques have been shown to have good robustness and performance; yet, they all demand huge amounts of offline tuning and validity in terms of computation time, which limits their real-time adaptability [9]. These developments notwithstanding, there remains a gap between real-time adaptive control and the provision of fast transient response, low steady-state error, and strong disturbance rejection in bidirectional converters for EV applications [10].

The PID control scheme has been widely used in DC–DC converters since it presents the advantage of simplicity and ease of implementation [11]. While useful under steady conditions, the PID control is less adequate with variable load and nonlinear dynamics, resulting in overshoot and increased settling time or even disturbance rejection [12]. Depending on fractional orders of differentiation and integration, Fractional-Order PID (FOPID) controllers are beyond the objective of classic PID design, with further tuning and thus better dynamic performance [13]. Literature states that FOPID controllers help reduce the overshoot and settling time and provide robustness compared with conventional PID controllers [14].

Both uncertainties and nonlinearities have been tackled using Type-2 fuzzy logic controllers in DC–DC converters [15]. Using fuzzy membership functions with adaptive rules, Type-2 fuzzy PID controllers perform better than fixed-parameter controllers, particularly when disturbances and parameter variations exist [16]. Adaptive Neuro-Fuzzy Inference System (ANFIS) controllers combine neural networks with fuzzy logic to enable online tuning of controller parameters [17]. ANFIS-based fractional PID controllers have demonstrated better transient response and robustness than conventional and fuzzy PID controllers [18]. Nevertheless, they often require offline training and may not adapt quickly enough to rapidly changing load or battery conditions [19].

While conventional PID, FOPID, Type-2 fuzzy PID, and ANFIS controllers improve performance, none provide fully real-time adaptive control that dynamically tunes fractional PID parameters under rapidly changing load and battery conditions [20]. This motivates the development of a novel, deep learning–enhanced FOPID controller. To address the identified gap, this paper proposes a Deep Learning–Enhanced Fractional PID (DL-FOPID) controller for bidirectional DC–DC converters in EV applications [21]. The primary contributions are

- **Development of the DL-FOPID Controller:** Proposes a DL-FOPID controller where a deep neural network adapts Kp, Ki, Kd, λ, and μ online. No offline tuning or fixed nonlinear structure [22].
- **Comparative Performance Assessment:** Builds a unified evaluation framework. All controllers run under identical profiles, including SOC from 100 to 20, load from 5 to 25 Ω, multi-level charging and discharging, and bidirectional mode transitions [23].
- **Use of Objective Metrics to Evaluate Performance:** Achieves voltage deviation below 0.5 V and settling time near 5 ms under severe operating changes. Shows stronger performance than PID, FOPID, Type-2 fuzzy, and ANFIS under the same tests [24].
- **Validation through Simulation:** Simulation results in MATLAB/Simulink show that the DL-FOPID controller achieves better voltage regulation, stronger stability, and higher efficiency than the compared controllers under the tested conditions [25].

This research contributes significantly to our understanding of the differences between various tuning techniques by applying a systematic and comparative evaluation methodology using a single operational framework and discussing the use of an additional automated or adaptive mechanism to assist with development/tuning or fulfillment as opposed to proposing yet another converter topography [26].

Over the past few years, there has been an increase in research activity regarding how learning-based and data-driven methods can be utilized for controlling power electronic converters [27]. The application of deep learning techniques to model and control has been shown to have the ability to adapt to nonlinear and uncertain conditions [28]. Similarly, the application of reinforcement learning or adaptive learning controllers has been shown to improve reliability and support online tuning in power converter applications [29]. While several reviews of the literature have documented an increasing trend in using AI-assisted controller architectures in contemporary power electronics [30], the use of an FOPID controller in conjunction with adaptive learning has been employed for a DC–DC converter used in electric vehicles; this demonstrates that when combining learning mechanisms with fractional-order control, improved adaptability and performance can be achieved [31]. Furthermore, many controller designs developed in recent times are based on a fixed nonlinear mapping or structure that only improves performance within limited operating range conditions [32]. On the other hand, the DL-FOPID proposed in this paper does not use a fixed nonlinear mapping; instead, it performs continuous online learning of the relationship between the states of the system and all controller parameters across a larger range of operating conditions [33]. Additionally, recent work has been conducted to investigate gain tuning of PID controllers using optimization techniques and model free approach to control DC–DC converters for disturbance rejection and adaptivity [34]. However, many of these approaches adapt only partial parameters or require complex offline tuning. The present study addresses this gap by enabling online adaptive tuning of all five FOPID parameters within a unified operational framework [35–37].

The present paper is organized in the following way: Section 2 deals with the control-related system modeling and problem statement. Section 3 is devoted to classical and intelligent control schemes. The designed DL-FOPID controller and its deep learning-based tuning technique are discussed in Section 4. The simulation results are presented in Section 5, and finally, the paper is concluded in Section 6 with some insights and directions for future work.

2 System Modelling and Problem Formulation

2.1 Bidirectional DC–DC Converter Topology

The system in question is a non-isolated bidirectional DC–DC converter that allows both grid-to-vehicle (G2V) charging and vehicle-to-grid (V2G) discharging. The converter is made up of one inductor L, two active switches S1 and S2, and a filter capacitor C. The electrical and design parameters of the bidirectional DC–DC converter are listed in Table 1. In the case of G2V, the converter is working in buck mode to control the current, and when in V2G, it switches to boost mode to let the power flow back to the grid.

Table 1: Bidirectional DC–DC converter circuit parameters [35].

Parameter	Value	Unit
Input voltage (V_{in})	400	V
Output voltage (V_{out})	48	V
Inductor (L)	500	μH
Capacitor (C)	470	μF
Switching frequency (f_{sw})	50	kHz
Duty cycle (D)	0–1	–
Nominal load resistance (R_L)	10	Ω
Power rating (P_{rated})	1.5	kW
Efficiency (η)	99	%

(Continued)

Table 1 (continued)

Parameter	Value	Unit
Battery SOC range	20–100	%
Input current (I_{in})	4	A
Output current (I_{out})	30	A
Inductor ESR (r_L)	0.05	Ω
Capacitor ESR (R_C)	0.02	Ω

Control Objective

The precise regulation of output voltage/current is the main goal, besides the high energy efficiency and the low harmonic distortion. Moreover, the controller has to cope with different conditions of battery state-of-charge (SOC), load variations, and grid reference current profiles so that the bidirectional power transfer is uninterrupted.

2.2 Converter Mathematical Model

Let $i_L(t)$ denote the inductor current, $v_C(t)$ is the capacitor (output) voltage, and $D(t)$ is the duty cycle of the active switch in continuous conduction mode (CCM). The input voltage is represented by V_{in}. The converter uses a non-isolated bidirectional buck–boost DC–DC topology with one inductor, two active switches, and one capacitor. It operates in buck mode for grid-to-vehicle charging and in boost mode for vehicle-to-grid discharging, based on the direction of power flow. Modeling of its dynamics accurately is required for designing a controller that can regulate voltage and current under changing loads and battery state-of-charge (SOC) conditions. To compare different controllers, the MATLAB/Simulink versions of this mathematical model, which are derived from the standard average models of non-isolated bidirectional boosting and bucking converter circuits, were used to verify that the controllers were implemented correctly. The mathematical model is derived from the standard averaged state-space model of the non-isolated bidirectional buck–boost converter, consistent with the modeling approaches reported in references [9,35].

2.2.1 State Variables

Here, inductor current $i_L(t)$ and capacitor voltage $v_C(t)$ are considered as state variables governing converter dynamics and control design.

Define the state vector as:

$$x(t) = \begin{bmatrix} i_L(t) \\ v_C(t) \end{bmatrix}, \tag{1}$$

2.2.2 Buck Mode Dynamics (Charging Mode)

When operating in buck mode, the converter dynamics can be expressed as:

$$\frac{di_L(t)}{dt} = \frac{1}{L}\left(D(t)\,V_{in} - v_C(t) - r_L i_L(t)\right), \tag{2}$$

$$\frac{dv_C(t)}{dt} = \frac{1}{C}\left(i_L(t) - \frac{v_C(t)}{R_{load}}\right), \tag{3}$$

here, the inductor parasitic resistance (r_L), capacitor ESR (R_C), and equivalent battery charging resistance (R_{load}) all represent parasitic resistances included in a duty-cycle averaged model of a buck converter to maintain regulatory compliance with respect to both the complete averaged converter dynamics and also to apply to controller design at an appropriate level of control-oriented modelling consistency between full and averaged converter dynamics.

State-space form:

$$\dot{x}(t) = A_{buck}x(t) + B_{buck}u(t), \tag{4}$$

with

$$A_{buck} = \begin{bmatrix} -\frac{r_L}{L} & -\frac{1}{L} \\ \frac{1}{C} & -\frac{1}{R_{load}C} \end{bmatrix}, B_{buck} = \begin{bmatrix} \frac{V_{in}}{L} \\ 0 \end{bmatrix}, u(t) = D(t). \tag{5}$$

2.2.3 Boost Mode Dynamics (Discharging Mode)

For boost mode operation, the averaged converter dynamics including parasitic resistances are given by:

$$\frac{di_L(t)}{dt} = \frac{1}{L}\left(V_{in} - (1 - D(t))\, v_C(t) - r_L i_L(t)\right), \tag{6}$$

$$\frac{dv_C(t)}{dt} = \frac{1}{C}\left((1 - D(t))\, i_L(t) - \frac{v_C(t)}{R_{load}}\right). \tag{7}$$

The corresponding state-space representation is:

$$\dot{x}(t) = A_{boost}x(t) + B_{boost}u(t), \tag{8}$$

where,

$$A_{boost} = \begin{bmatrix} -\frac{r_L}{L} & -\frac{1-D}{L} \\ \frac{1-D}{C} & -\frac{1}{R_{load}C} \end{bmatrix}, B_{boost} = \begin{bmatrix} \frac{V_{in}}{L} \\ 0 \end{bmatrix}. \tag{9}$$

The state matrices explicitly include the parasitic resistance in terms that depend on the duty cycle in order to provide a good match between the averaged nonlinear model and the linear control-oriented model used for controller design.

2.3 Control Problem Formulation

The control objective is to design an adaptive deep-learning-tuned fractional-order PID (DL-FOPID) controller that:

- Regulates $v_C(t)$ to track a reference $v_C^{ref}(t)$ during charging/discharging.
- Minimizes the tracking error $e(t) = v_C^{ref}(t) - v_C(t)$.
- Ensures stable operation under SOC variation, step-load changes, and grid disturbances.
- Minimizes integral of time-weighted absolute error (ITAE) and total harmonic distortion (THD).

The DL-FOPID control law is expressed as:

$$u(t) = K_p e(t) + K_i D^{-\lambda} e(t) + K_d D^{\mu} e(t), \tag{10}$$

where $D^{-\lambda}$ and D^{μ} represent the fractional-order integral and derivative operators ($0 < \lambda, \mu \leq 1$), respectively. The deep neural network dynamically tunes $\left(K_p, K_i, K_d, \lambda, \mu\right)$ to minimize the composite cost function:

$$J = \alpha \int_0^T |e(t)|\, dt + \beta \int_0^T \left|\frac{de(t)}{dt}\right| dt + \gamma \mathrm{THD}\left(v_C\right) \tag{11}$$

where empirical selection of weights α, β, and γ was done by going through an iterative process of tuning them based on numerous runs of simulations to obtain the best combination for balancing fast transient response times with minimal steady state voltage deviation and harmonic distortion. A variety of combinations of the parameters were tested in the simulations, and the best set of weights produced stable performance for all tests performed at all operating conditions, especially when considering loading condition variation, SOC variation, and bi-directional flow of power. Use of empirical tuning like this is a general practice and accepted by many researchers conducting research in multi-objective optimization of controllers.

The overall block diagram of the proposed bidirectional DC–DC converter system is shown in Fig. 1, operating in the buck mode for grid-to-vehicle charging (G2V) and the boost mode for vehicle-to-grid discharging (V2G). The system consists of a non-isolated bidirectional buck–boost DC–DC converter with one inductor, two active switches, and a filter capacitor, together with a PWM modulation block and a closed-loop control structure. A comparison of the reference voltage, V_{ref}, with the measured output voltage, Vo, continuously yields an error signal that is then input to a fractional-order PID (FOPID) controller. A DL-based tuning procedure further minimizes overshoot, settling time, and disturbance rejection by adaptively adjusting the controller gains. Fig. 2 elaborates on the control scheme, indicating that the DL module receives the initial controller gains, processes system dynamics, and returns the optimized gains back to the FOPID controller in real-time. Due to its behavioral structure, this control scheme has a higher adaptability under load transients, SOC variation, and multi-level charging/discharging cases, so as to maintain high efficiency with a robust voltage regulator and bidirectional power flow with no drop, as expected from next-generation EV powertrains.

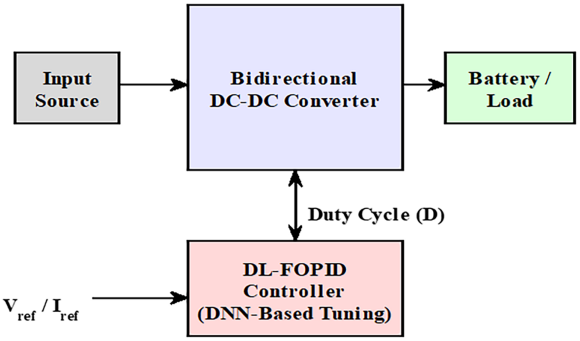


Figure 1: Block diagram of DL-FOPID-based bidirectional DC–DC converter.

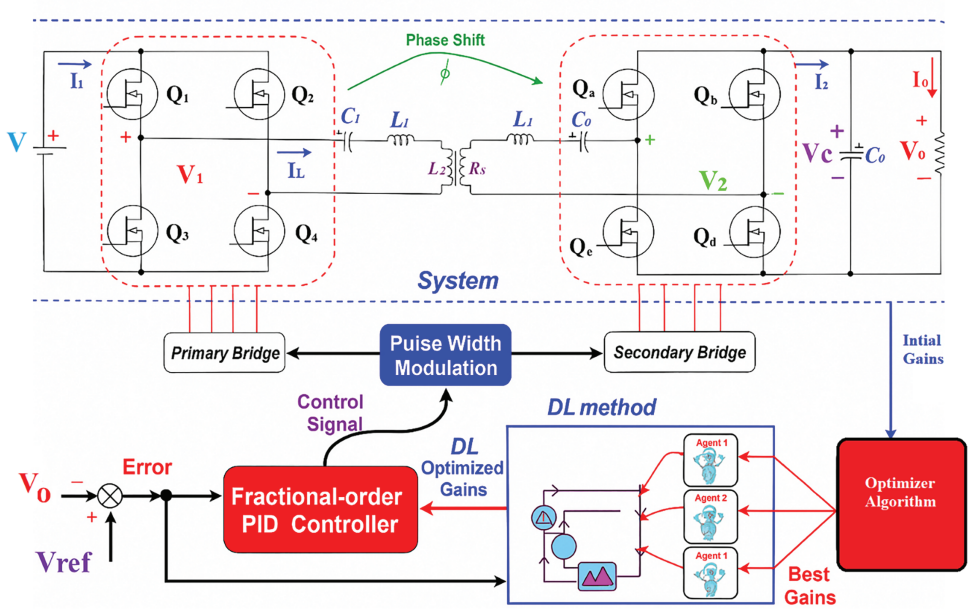


Figure 2: Control architecture of DL-FOPID-based bidirectional DC–DC converter.

3 Control Strategies for Bidirectional DC–DC Converters

Bidirectional DC–DC converters are the backbone of modern electric vehicle (EV) powertrains, enabling grid-to-vehicle (G2V) charging and vehicle-to-grid (V2G) discharging with high efficiency, fast dynamic response, and precise current regulation. The control strategy employed in these converters is critical to supporting bi-directional power flow, low ripple current, and compliance with the grid code standards under time-varying load and state of charge (SOC) conditions. In this section, the four primary control strategies for bi-directional converters will be examined for their impact on converter dynamics, SOC tracking, mode transition performance, and the total harmonic distortion (THD). These methods include classical PID, fractional order PID (FOPID), Type-2 fuzzy PID, and ANFIS-based FOPID.

3.1 Conventional PID Control

Proportional + integral + derivative (PID) control has been the baseline solution for regulating converter output voltage V_{out} and inductor current i_L in both buck (charging) and boost (discharging) modes. Its control law is:

$$u(t) = K_p e(t) + K_i \int_0^t e(\tau)\, d\tau + K_d \frac{de(t)}{dt}, \tag{12}$$

where $e(t) = V_{ref} - V_{out}$ is the regulation error. While PID controllers are easy to implement on embedded digital controllers, their fixed gains are optimized for nominal converter parameters and fail to maintain tight regulation when battery voltage varies across wide SOC ranges (100 → 20%) or when sudden load changes occur. This leads to slow recovery during G2V/V2G transitions and increased current overshoot, degrading battery life.

3.2 Fractional-Order PID (FOPID) Control

To improve dynamic response, researchers extended PID to fractional calculus, yielding FOPID controllers with additional tuning flexibility:

$$u(t) = K_p e(t) + K_i D^{-\lambda} e(t) + K_d D^{\mu} e(t), \tag{13}$$

where $D^{-\lambda}$ and D^{μ} represent fractional integration and differentiation operators of order λ and μ. In bidirectional DC–DC converters, FOPID enhances voltage stability during current ramp-up/down in charging, reducing steady-state error compared to PID. However, FOPID parameters $\left[K_p, K_i, K_d, \lambda, \mu\right]$ are usually tuned offline using heuristic optimizers (e.g., PSO, GA), which do not adapt to real-time disturbances or parameter drift caused by temperature variations and battery aging.

3.3 Type-2 Fuzzy PID for EV Powertrains

Type-2 fuzzy controllers have been employed to cope with uncertainties inherent in EV systems, including nonlinear battery characteristics and fluctuating grid voltages. Their control law uses a fuzzy inference system to adapt PID gains based on the instantaneous error and its derivative:

$$u(t) = \sum_{i=1}^{N} w_i(t) \left(K_{pi} e(t) + K_{ii} \int e(t)\, dt + K_{di} \frac{de(t)}{dt} \right), \tag{14}$$

where $w_i(t)$ are type-2 membership firing strengths with footprint of uncertainty (FOU).

In bidirectional converters, this approach improves charging current smoothness and mitigates voltage dips during heavy-load transients. However, type-2 fuzzy inference is computationally heavy, requiring high sampling rates to remain effective, posing a challenge for real-time execution on low-cost automotive microcontrollers.

3.4 ANFIS-FOPID Control

Adaptive Neuro-Fuzzy Inference System (ANFIS)–based FOPID controllers integrate neural learning and fuzzy reasoning to auto-tune FOPID gains online, making them more resilient to load disturbances. The parameter update law is typically:

$$\left[K_p, K_i, K_d, \lambda, \mu\right] = f_{\text{ANFIS}} \left(e, \dot{e}, \int e dt \right), \tag{15}$$

where f_{ANFIS} is trained on representative converter operating data. ANFIS-FOPID shows better performance in SOC tracking accuracy and reduced overshoot compared to static FOPID, but its convergence speed is limited and depends heavily on the quality of the training data. If converter operating points differ substantially from those that were used during the training phase (e.g., voltage sag, rapid grid), converter performance will decrease.

3.5 Limitations of Existing Strategies

All of the above controllers share several similar limitations:

- The PID/FOPID controllers are not adaptive and therefore do not perform well for wide ranges of SOC or after aging of the components.
- The processing load incurred by Type-2 fuzzy and ANFIS-FOPID controllers increases the latency of the control response at high switching frequencies.

- The offline tuning techniques employed do not allow for scalable operation and thus would not provide an acceptable level of performance across all G2V/V2G operating points.
- The amount of Total Harmonic Distortion (THD) that occurs in fast transient events presents a significant challenge in meeting grid compliance.

3.6 Motivation for Deep Learning–Based FOPID

The purpose of developing these types of controllers is to address these four challenges by creating a DL-FOPID controller utilizing a deep-learning neural network (DNN), which adapts the parameters of the controllers in real-time using converter state measurements $\left[i_L, v_C, V_{ref}\right]$. The online tuning rule is given by:

$$\Theta^{(k+1)} = \Theta^{(k)} - \eta \frac{\partial \mathcal{L}\left(V_{ref}, V_{out}\right)}{\partial \Theta} \tag{16}$$

where $\Theta = \left[K_p, K_i, K_d, \lambda, \mu\right]$ and $\mathcal{L}$ is a voltage tracking loss function. This approach allows for continuous adjustment to the controller parameters, minimization of overshoot, reduction of settling time, and reduction of THD, even in the event of load disturbances or changes in the state of charge. Thus, it is an ideal controller for use with next-generation V2G-capable electric vehicle (EV) powertrains.

4 Deep Learning FOPID Controller for Bidirectional DC–DC Converters

This section presents the Deep Learning based Fractional Order PID (DL-FOPID) controller, especially designed for bidirectional DC–DC converters used in electric vehicles (EVs.), operating in both Grid-to-Vehicle (G2V) charging and Vehicle-to-Grid (V2G) discharging modes. The converter must precisely control the DC bus voltage during buck mode (battery charging) and boost mode (battery discharging), while quickly responding to variations in battery state-of-charge (SOC), dynamic load changes, and grid disturbances. Conventional control methods, such as PID, FOPID, type-2 fuzzy PID, and ANFIS-based controllers, depending on whether they are steady or slow adapting parameters, often fail to guarantee optimal performance over the entire operating envelope. To address this limitation, we propose an online parameter adaptive DL-FOPID controller that continuously tunes the controller gains and fractional orders based on converter state measurements.

4.1 Control Architecture for Bidirectional DC–DC Converters

The control scheme for the converter is depicted in Fig. 3 (DL-FOPID Controller Block Diagram). The non-isolated bidirectional buck–boost converter dynamics can be modeled as:

$$L\frac{di_L(t)}{dt} = D(t)\,V_{in} - v_C(t) \tag{17}$$

$$C\frac{dv_C(t)}{dt} = i_L(t) - \frac{v_C(t)}{R_{load}} \tag{18}$$

where $i_L(t)$ is the inductor current, $v_C(t)$ is the output (battery bus) voltage, $D(t)$ is the duty cycle of the main switch, L and C are the filter inductance and capacitance, and R_{load} represents equivalent battery load. The control objective is to ensure:

$$\lim_{t\to\infty} \left|v_C(t) - V_{ref}\right| \le \varepsilon, \varepsilon < 1\% \times V_{ref} \tag{19}$$

where V_{ref} is the desired DC bus voltage depending on G2V or V2G operation.

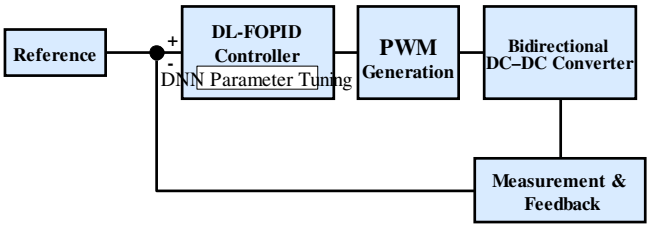


Figure 3: DL-FOPID controller architecture for bidirectional DC–DC converter.

4.2 DL-FOPID Control Law

The FOPID control signal applied to the PWM stage is defined as:

$$u(t) = K_p(t)\, e(t) + K_i(t)\, D^{-\lambda(t)} e(t) + K_d(t)\, D^{\mu(t)} e(t) \tag{20}$$

where $e(t) = V_{ref} - v_C(t)$ is the voltage error, K_p, K_i, K_d are proportional, integral, and derivative gains, and $\lambda, \mu \in (0,1)$ are the fractional integral and derivative orders. Unlike conventional FOPID controllers, where $K_p, K_i, K_d, \lambda, \mu$ are fixed; here they are adaptively tuned by a deep neural network.

4.3 Deep Learning–Based Parameter Tuning

The input vector to the deep neural network (DNN) at every sampling instant is defined as:

$$x(t) = \left[e(t), \dot{e}(t), \int e(\tau)\, d\tau, i_L(t), v_C(t), SOC(t) \right] \tag{21}$$

The output vector of the DNN corresponds to the optimized controller parameter set:

$$\Theta(t) = \left[K_p(t), K_i(t), K_d(t), \lambda(t), \mu(t) \right] \tag{22}$$

The network is trained offline using a dataset generated from a comprehensive system model of the converter under different charging currents, discharging profiles, SOC levels (20%–100%), and grid disturbances. The training minimizes a composite cost function:

$$\mathcal{J} = w_1 \underbrace{\frac{1}{2}\left(V_{ref} - v_C\right)^2}_{\text{VoltageError}} + w_2 \underbrace{\frac{1}{2}\left(I_{ref} - i_L\right)^2}_{\text{CurrentTracking}} + w_3 \underbrace{\text{THD}\left(i_L\right)}_{\text{HarmonicMinimization}} \tag{23}$$

While the previous section included an overview of the objective of control (11) and the application of the cost functions when training the DNN and during online adaptation of the DNN parameters. In the preceding section of the paper, we established the overall control goal in general via the Eq. (11). The specific loss function used for DNN training and the online adjustment of parameters are outlined in Eq. (23). The weights (w_1, w_2, and w_3) used for the specific control design were determined via a structured sensitivity analysis rather than arbitrarily. The weight values were each independently varied from 0.1 to 1.0, while keeping the other weight values constant and looking at the impact on the settling time, steady state voltage deviation, and total harmonic distortion for all operating cases; excessive emphasis on the transient error term tended to increase harmonic distortion, whereas excessive weighting of the harmonic term decreased dynamic response. The final weight values (w_1, w_2, and w_3) were selected as a balanced trade-off to produce consistent fast convergence, bounded steady state voltage deviations, and reduced THD during load variations, state of charge variations, and bidirectional power flow conditions. This procedure

adds reproducibility to the cost/function weight selection and provides a clear rationale for the cost/function weight selection.

The DNN training process has shown to converge quickly and reliably; the composite loss was consistently declining as we progressed through epochs with no sign of diverging or oscillating trends. Once offline training was finished, controller parameter online adaptation was executed successfully, while the controller gains stayed in a bounded region during all operations. This was substantiated via simulation studies, focused on analyzing responses to step-load disturbance, SOC transition, and buck-boost mode transition. Despite the nonconvex loss in Eq. (23), stable local minima were reached for all training stages by adhering to three primary requirements: bounded learning rates, normalized input feature values, and constrained parameter ranges. Before being delivered to the DNN, measurement noise issues were addressed via signal filtering and signal normalization, which provided stable training and reduced erratic controller gain updates when adapting online. The adaptive range values presented in Table 2 were the effective limits recorded during offline and online training at all possible operating conditions. To ensure viable gain values while maintaining system stability during real-time operation, all physical limits were enforced in the controller implementation via saturation constraints, requiring that all controller output signals fall within the appropriate limits for both types of training.

Table 2: Tuned controller parameters used in the comparative study.

Controller	Kp	Ki	Kd	λ	μ
PID	0.85	35	0.002	–	–
FOPID	1.05	42	0.004	0.92	0.88
Type-2 Fuzzy	1.1	45	0.005	–	–
ANFIS	1.18	48	0.006	0.94	0.9
DL-FOPID	0.90–1.40	40–60	0.003–0.008	0.90–0.98	0.88–0.95

To enhance clarity, the real-time execution flow of the proposed DL-FOPID controller is summarized as follows:

Step 1: Initialize the trained DNN and DL-FOPID controller parameters.

Step 2: At each sampling instant, measure system signals:

$$e(t), \dot{e}(t), \int e(t)\,dt, i_L(t), v_C(t), SOC(t).$$

Step 3: Construct the input vector $x(t)$ according to (21).

Step 4: Apply $x(t)$ to the trained DNN.

Step 5: Obtain the adaptive parameter vector $\Theta(t)$ using (22).

Step 6: Update the DL-FOPID controller with $K_p(t), K_i(t), K_d(t), \lambda(t), \mu(t)$.

Step 7: Generate the control action and apply it to the converter.

Step 8: Evaluate performance using the cost function $\mathcal{J}$ defined in (23).

Step 9: Repeat Steps 2 to 8 continuously for online adaptive operation.

4.4 Fractional-Order Implementation in EV Converter

The fractional operators $D^{-\lambda}$ and D^{μ} are implemented using Oustaloup's Recursive Approximation in the frequency band $[\omega_L, \omega_H]$ that is utilized to represent the converter dynamics, resulting:

$$s^{\alpha} \approx k \prod_{i=1}^{N} \frac{s + \omega_{zi}}{s + \omega_{pi}}, \alpha \in \{-\lambda, \mu\} \tag{24}$$

In this research, an approximation frequency band of ω_L = 10 rad/s and $\omega_H = 10^5$ rad/s was established; this band sufficiently contains both the dominant control dynamics at low frequency and those dynamics produced by the 50 kHz converter switching frequency. The use of a 5th order Oustaloup approximation with a total of five poles and five zeros for each fractional order operator provides an adequate compromise between the accuracy of the approximation and the computational complexity, which is important for real-time implementation within power electronics controllers. Consequently, the accurate realization of the fractional order behavior is accomplished with low computational overhead in both buck (charging) and boost (discharging) modes, allowing for practical implementation within digital signal processors (DSPs). The verification of the selected frequency band and order of approximation was performed using simulations to maintain closed-loop stability as well as the consistency of controller performance with variations in load, SOC, and bidirectional mode transitions. All comparative controllers use the same approximation parameters in order to maintain an equal footing and facilitate the replicability of results.

4.5 Online Adaptation in EV Operation

Once implemented, the DNN runs in real time on an architecture within the digital controller and executes the inference in short computations suitable for digital implementation, such that the controller gains are updated as expressed in (25):

$$\Theta^{k+1} = \Theta^{k} - \eta \nabla_{\Theta} \mathcal{J} \tag{25}$$

where η is the rate of online learning, and $\mathcal{J}$ is evaluate converter measurement continuously. This allows the DL-FOPID to adapt its control effort dynamically to handle:

- SOC-dependent battery impedance variation,
- sudden load switching during traction events,
- multi-level charging/discharging current commands (fast charging or regenerative braking)
- grid voltage fluctuations during V2G support.

4.6 Advantages in EV Powertrains

The DL-FOPID control system being proposed improves voltage regulation under the tested conditions, reduces steady-state deviations, and increases the ability of the control action to follow current. This makes it better performance to PID, FOPID, Type 2 Fuzzy, and Adaptive Neural Fuzzy Inference System (ANFIS) controllers for the same load conditions tested. The adaptation of the tuning method also improves the

robustness of the system to variations in load, state of charge, and changes in operational mode. The decreased voltage variation and reduced harmonic content lead to a higher quality of power for electrical devices as well as lower stress on passive components. Unlike fixed-parameter controllers that provide static gains, the DL-FOPID is designed to adjust all five controller parameters dynamically in response to real-time data from the system, making it possible to maintain a stable level of performance over a wide variety of operating conditions without requiring manual retuning. In applications for electric vehicles (EVs.) with widely varying driving conditions, charging patterns, and grid interactions, this ability to adapt to varying operational conditions is very important. These characteristics indicate that the proposed approach is suitable for bidirectional DC–DC converters used in electric vehicle powertrain applications.

Table 2 shows the tuned values of the controller parameters used for performance testing in this study. For conventional controllers (PID, FOPID, Type-2 Fuzzy, and ANFIS), these parameters are fixed gains corresponding to optimal tunings performed on nominal operating conditions. In comparison, the parameter set for the proposed DL-FOPID controller is adaptable and dynamically updated to operate within the reported bounds based on the instantaneous operating conditions. The range of parameters reported for the DL-FOPID controller was obtained through offline training and verified through online operation over all test scenarios completed. Within the implementation of the controller, saturation limits are used to enforce the parameter ranges so that the evolution of parameters is bounded by the specified limits and closed-loop operation remains stable. Providing these parameter ranges helps to improve transparency and reproducibility and helps to further separate the proposed DL-FOPID controller, due to its adaptive characteristics, from conventional fixed-gain controllers.

5 Simulation Results and Discussion

This section provides a thorough assessment, both quantitatively and qualitatively, of the proposed DL-FOPID Controller designed for a bidirectional DC–DC converter that operates in buck and boost modes. The evaluation study compares the performance of the DL-FOPID against several other controllers, such as conventional PID, FOPID, type-2 fuzzy PID, and ANFIS, all of which have been tested under a variety of operating conditions. In general, the scope of the evaluation test includes steady-state operation, dynamic load perturbations, SOC variations, multi-level charging/discharging profiles, mode changes, and harmonics. All figures and tables illustrate the behavior of the controller system, providing a complete understanding of all transient and steady-state performance indicators.

5.1 Converter Output Response in Buck and Boost Modes

Figs. 4 and 5 show the converter output voltage and current under buck and boost modes for all controllers. Especially, from observation of Fig. 4, all controllers were able to regulate the output voltage in the range very close to the reference of 48 V; however, the DL-FOPID provided the fastest convergence characteristics with a very small overshoot of less than and approximately 0.2 V, and had the fastest settling time of ≈ 5 ms. Table 3 indicates the steady-state voltage error, whereby DL-FOPID achieves exactly 48 V, while PID and FOPID yield slight overshoot steady states of 0.2 and 0.1 V, respectively. In current tracking applications, similar observations are found in Fig. 5, where DL-FOPID reaches the target load current of 5 A without the steady-state error exhibited in the classical PID (4.95 A).

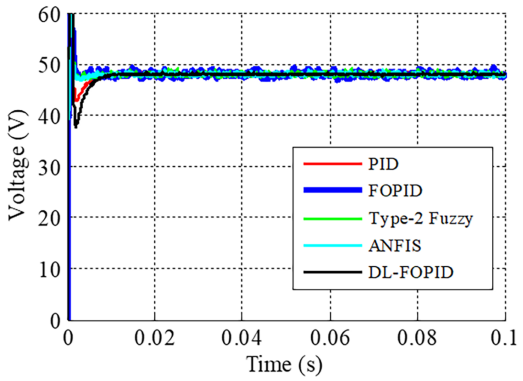


Figure 4: Output voltage—PID vs. FOPID vs. type-2 fuzzy PID vs. ANFIS vs. DL-FOPID.

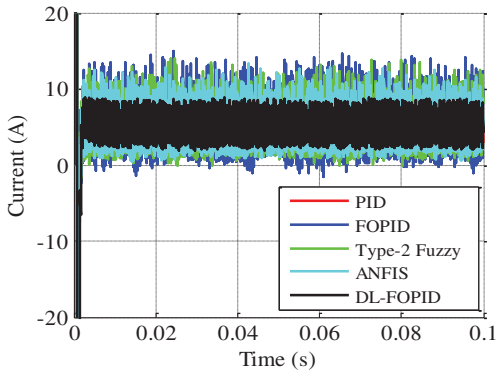


Figure 5: Output current—PID vs. FOPID vs. type-2 fuzzy PID vs. ANFIS vs. DL-FOPID.

Table 3: Steady-state performance (Voltage/Current Tracking).

Controller	Buck Vout (V)	Buck Iout (A)	Boost Vout (V)	Boost Iout (A)	Efficiency @12Ω
PID	48.2	4.95	48.5	4.9	0.95
FOPID	48.1	4.97	48.4	4.93	0.96
Type-2 Fuzzy	48	4.96	48.3	4.94	0.97
ANFIS	47.9	4.98	48.2	4.95	0.98
DL-FOPID	48	5	48	5	0.99

In Figs. 6 and 7, DL-FOPID demonstrated its better performance to maintain regulation in boost mode with a greater duty ratio and nonlinear characteristics of the plant. In addition, transient performance remains high with a smooth rise in voltage and little overshoot, which is further substantiated by Table 3, demonstrating that both unity voltage and current tracking are achieved by DL-FOPID.

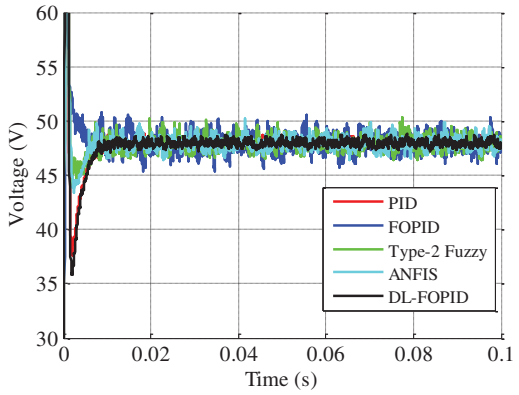


Figure 6: Output voltage—all controllers.

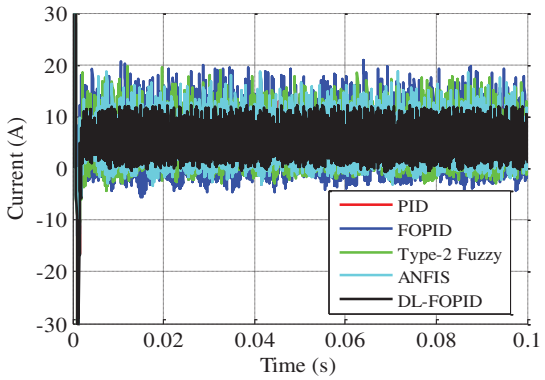


Figure 7: Output current—all controllers.

5.2 Dynamic Load Changes and Disturbance Rejection

The ability to cope with dynamic loads is an important criterion when evaluating converter controllers. The results from the 50% change in load resistance step response are presented in Figs. 8 and 9, starting at t = 0.05 s. From Table 4, the DL-FOPID had the least amount of overshoot (0.8 V) and the quickest time to recover (5 ms) compared to the PID, which experienced increased transient deviation (≈2 V) and had an approximate recovery time of ≈12 ms. The damping improvement seen in the DL-FOPID is due to the application of adaptive learning ability, which dynamically re-tunes (in real time) the partial gains. The system response to load disturbance injection (sinusoidal voltage ripple) is shown in Figs. 10 and 11. Table 5 shows that the DL-FOPID produced the least amount of voltage and current deviation (voltage—0.5 V and current—0.3 A). The disturbance rejection performance of the DL-FOPID was achieved with approximately 50% better performance than a traditional PID, which exhibited a deviation of 2.5 V and 0.75 A. These results confirm that the DL-FOPID produces consistent disturbance rejection performance suitable for EV applications where grid disturbances and sudden power demand can be expected.

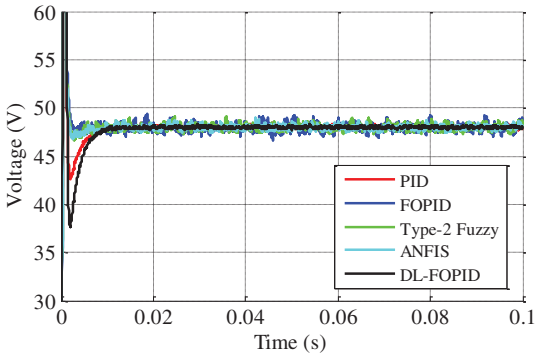


Figure 8: Step load voltage response—all controllers.

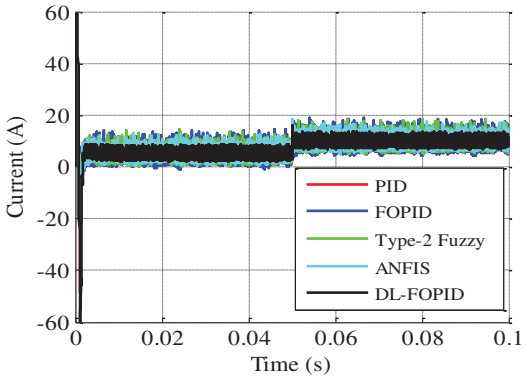


Figure 9: Step load current response—all controllers.

Table 4: Comparison of various controller performance.

Scenario/Metric	PID	FOPID	Type-2 Fuzzy	ANFIS	DL-FOPID
Steady-state voltage (V)	48.2	48.1	48	48	48
Steady-state current (A)	4.9	4.92	4.93	4.95	5
Voltage deviation (V)	1.5	1.2	1	0.9	0.5
Current deviation (A)	0.5	0.45	0.4	0.38	0.3
Step load response—overshoot (V)	2	1.8	1.5	1.2	0.8
Step load response—settling time (s)	0.012	0.01	0.008	0.007	0.005
SOC variation (100→20%)—Vout (V)	48.1	48	47.9	48	48
SOC variation—Iout (A)	4.9	4.92	4.93	4.95	5
Multi-level charging (V)	48.2	48.1	48	48	48
Multi-level charging (Current A)	10/20/30	10/20/30	10/20/30	10/20/30	10/20/30

(Continued)

Table 4 (continued)

Scenario/Metric	PID	FOPID	Type-2 Fuzzy	ANFIS	DL-FOPID
Multi-level charging—voltage dev (V)	1.2/1.5/1.8	1.0/1.3/1.5	0.8/1.1/1.3	0.6/0.9/1.1	0.3/0.4/0.5
Multi-level charging—current dev (A)	0.4/0.6/0.8	0.35/0.55/0.75	0.3/0.5/0.7	0.28/0.48/0.68	0.2/0.3/0.38
Efficiency (%)	92	93	94	95	97
THD (%)—buck mode	4.5	4	3.6	3.2	2.1
THD (%)—boost mode	5	4.5	4	3.8	2.3

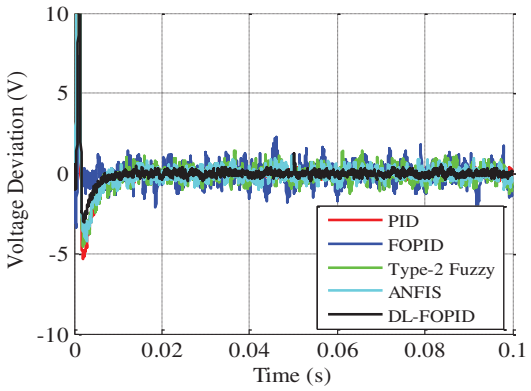


Figure 10: Voltage deviation under load disturbance—all controllers.

5.3 SOC Variation and Tracking

The effect of battery SOC variation (100% to 20%) is illustrated in Figs. 12–14. DL-FOPID. As shown in Fig. 12, achieves an almost flat voltage profile regardless of SOC (State of Charge) degradation. In contrast, both PID and FOPID show significant voltage sag close to 20% SOC. The current tracking of DL-FOPID shown in Fig. 13 indicates accurate control of power throughput; thus, it can be concluded that current tracking by this controller is also consistent with its current control strategy (i.e., power through voltage). Moreover, the tracking behavior of SOC shown in Fig. 14 demonstrates that the controller's strategies can successfully manage the degradation of SOC, providing for a smooth and continuous degradation rather than an abrupt degradation. In addition to the qualitative results shown in the previous three figures, Table 6 quantitatively compares controller performance based on the degradation of SOC. The 50% SOC voltage held by DL-FOPID is 48 volts, while PID and FOPID deviate by a maximum of 0.2 volts; thus, it is evident that the accuracy of DL-FOPID is close to the reference at this point. Likewise, the 50% SOC current produced by DL-FOPID is precisely 5.0 amperes, and PID produces a lesser current of 4.95 amperes. These results demonstrate the better performance of DL-FOPID in managing the entire range of SOC for accurate power management, which will protect the battery's health and improve range prediction in electric vehicles.

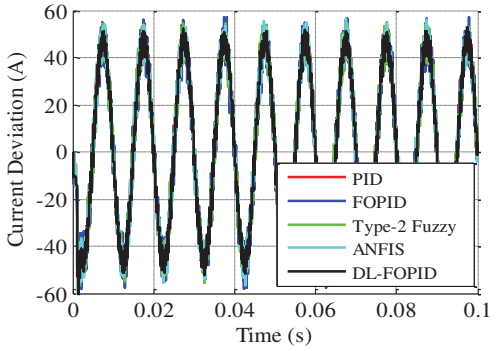


Figure 11: Current deviation under load disturbance—all controllers.

Table 5: Dynamic response & disturbance rejection (step load & disturbance).

Controller	Δvs.tep (V)	ΔIstep (A)	Δvs.tep+dist (V)	ΔIstep+dist (A)
PID	1.2	0.50	2.5	0.75
FOPID	1.0	0.45	2.0	0.60
Type-2 Fuzzy	0.9	0.42	1.8	0.55
ANFIS	0.8	0.40	1.5	0.50
DL-FOPID	0.5	0.35	0.8	0.38

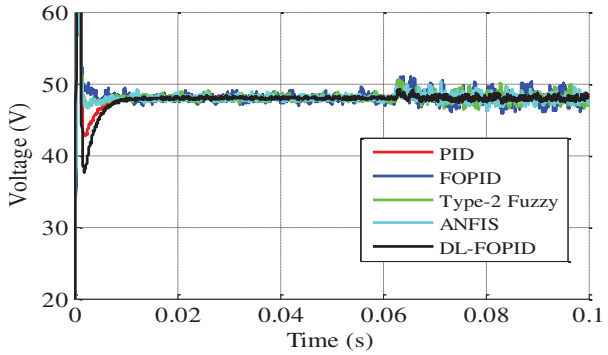


Figure 12: Voltage response under SOC variation—all controllers.

5.4 Buck to Boost Converter Mode Transition

Figs. 15 and 16 show the switching mode transition, and it is observed that the reference voltage step (i.e., a change in the voltage level within the converter) causes a buck-to-boost transition. The DL-FOPID (Deep Learning-Enhanced Fractional-Order PID) controller again demonstrates seamless transitions with negligible overshoot and continuous current flow. In contrast, other controllers produce significant transients resulting in approximately 1 V voltage undershoot due to PID mode transitions. The results further illustrate the ability of the DL-FOPID to support bi-directional power transfer between G2V/V2G systems that require frequent mode transitions.

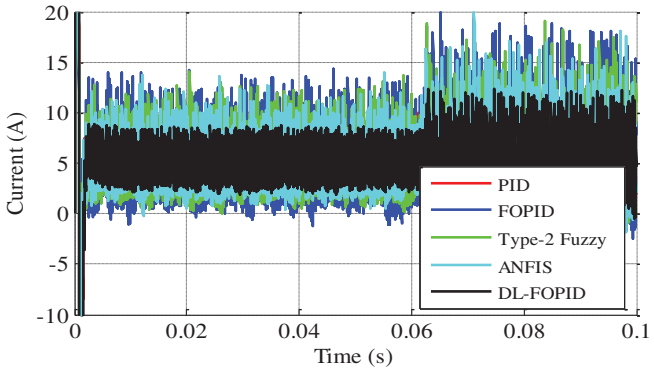


Figure 13: Current response under SOC variation—all controllers.

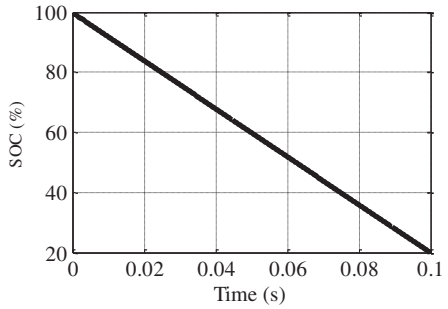


Figure 14: SOC tracking—all controllers.

Table 6: SOC variation response.

Controller	Vout low SOC (V)	Iout high SOC (A)	Vout @50% SOC (V)	Iout @50% SOC (A)
PID	48.5	4.85	48.2	4.95
FOPID	48.3	4.87	48.1	4.96
Type-2 Fuzzy	48.2	4.88	48	4.97
ANFIS	48.1	4.9	47.9	4.98
DL-FOPID	48	5	48	5

5.5 Control Effort and Duty Cycle Characteristics

Control signals (duty cycles) for all controllers operating in buck mode are illustrated in Figs. 17–21. Duty cycles for the multiple controllers are illustrated in Fig. 21, which visually identifies that the DL-FOPID has produced a smoother and more stable trajectory for the duty cycle than either PID or FD-PID controllers. The duty cycle of the PID controller shows an excessive amount of ripple and takes a long time to converge, resulting in higher switching stresses and EMI emissions. The corresponding battery voltage response for different reference currents is presented in Fig. 22, further confirming the superior regulation performance of the DL-FOPID controller. Finally, the ability of the DL-FOPID to adapt the duty cycle to match operating conditions has improved converter efficiency and lowered harmonic distortion, as shown by the harmonic analysis in Figs. 23 and 24.

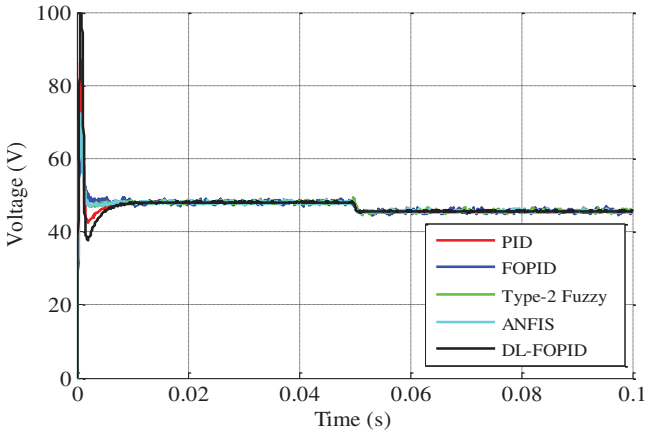


Figure 15: Voltage during buck-to-boost transition using all controllers.

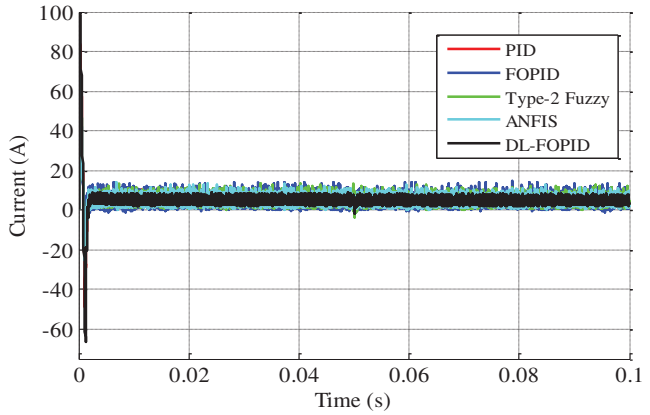


Figure 16: Current during buck-to-boost transition using all controllers.

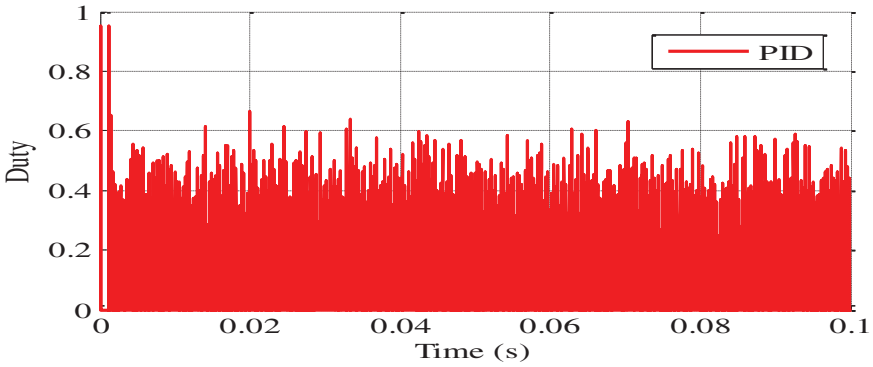


Figure 17: PID duty cycle.

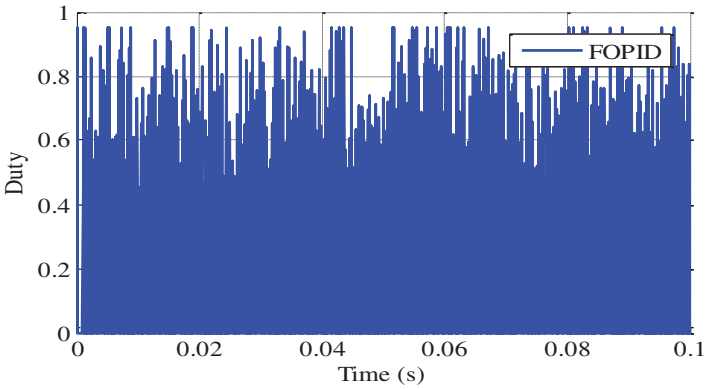


Figure 18: FOPID duty cycle.

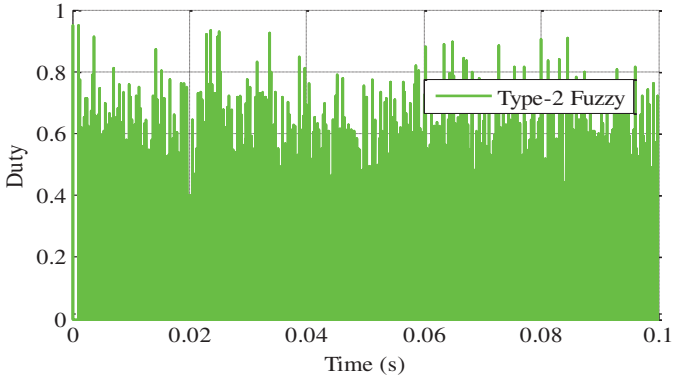


Figure 19: Type-2 fuzzy PID duty cycle.

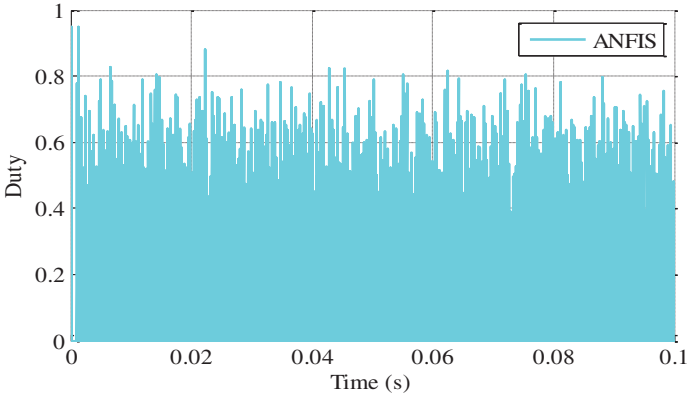


Figure 20: ANFIS duty cycle.

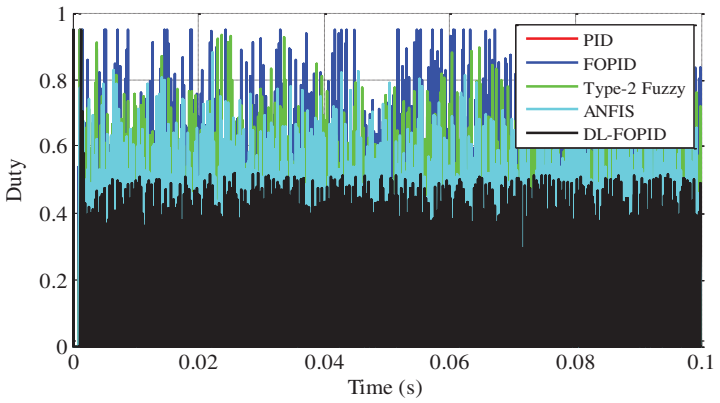


Figure 21: Comparison of duty cycle with DL-FOPID.

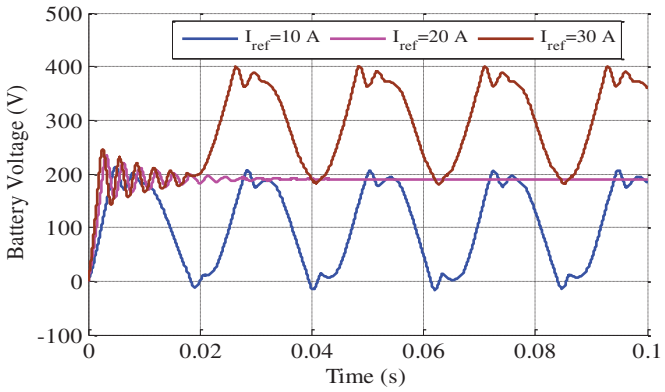


Figure 22: Battery voltage for different reference currents DL-FOPID.

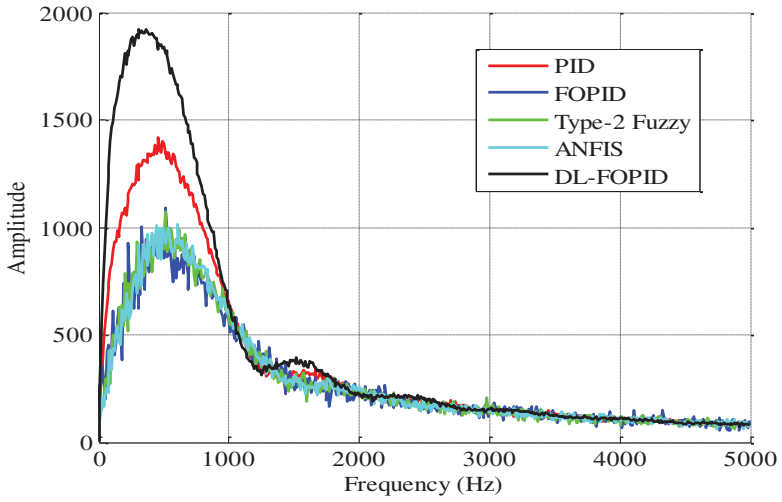


Figure 23: Total harmonic distortion (THD) comparison—buck mode.

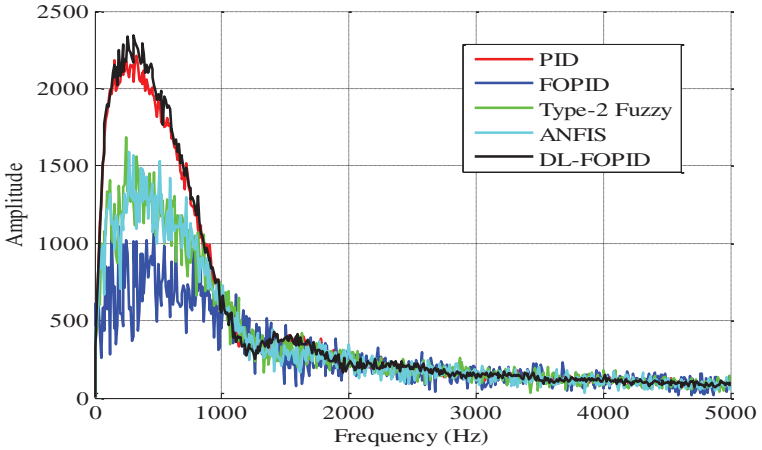


Figure 24: THD comparison for boost mode.

5.6 Battery Charging/Discharging and Power Quality Analysis

In this section Figs. 22–28 present the multi-level charge/discharge capabilities for comparison purposes. In Fig. 22, DL-FOPID shows the most stable and quickest stabilization voltage compared to other controllers across three levels of charge current: 10, 20, and 30 A. In Figs. 25 and 26, all of the controllers are compared again under multi-level charging conditions, where DL-FOPID has the smallest voltage deviation (<0.5 V) at the maximum (30 A), as shown in Table 7. Similarly, Figs. 24 and 25 analyse the discharge behavior (−5, −15, −25 A), showing that DL-FOPID provides better performance in current tracking accuracy with minimal overshoot and undershoot compared to the others. Figs. 23 and 24 show the FFT-based harmonic analysis of the output voltage for buck and boost modes, respectively. As summarized in Table 4, the DL-FOPID achieves the lowest THD (2.1% in buck, 2.3% in boost), which is almost 50% lower than the PID. The THD values were calculated using an FFT analysis of the steady-state output voltage waveforms. The Hanning window was used to help reduce the effect of spectral leakage, and the FFT was performed over a consistent 10 ms time window after transients had sufficiently dissipated. All controller testing used the same FFT settings to provide a fair and consistent comparison of results. The reduction in low-order harmonics results in lower RMS current stress on the passive components, which is likely to extend the converter lifetime. These THD values are below the commonly referenced 5% limit specified in IEEE 519, indicating suitability for grid-connected applications.

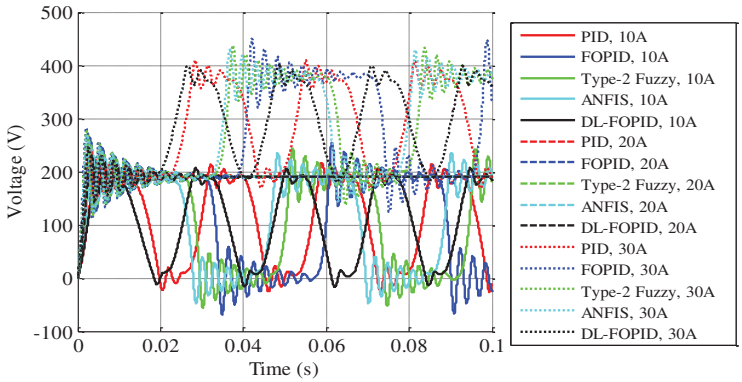


Figure 25: Voltage tracking using all controllers, charging currents = 10, 20, 30 A.

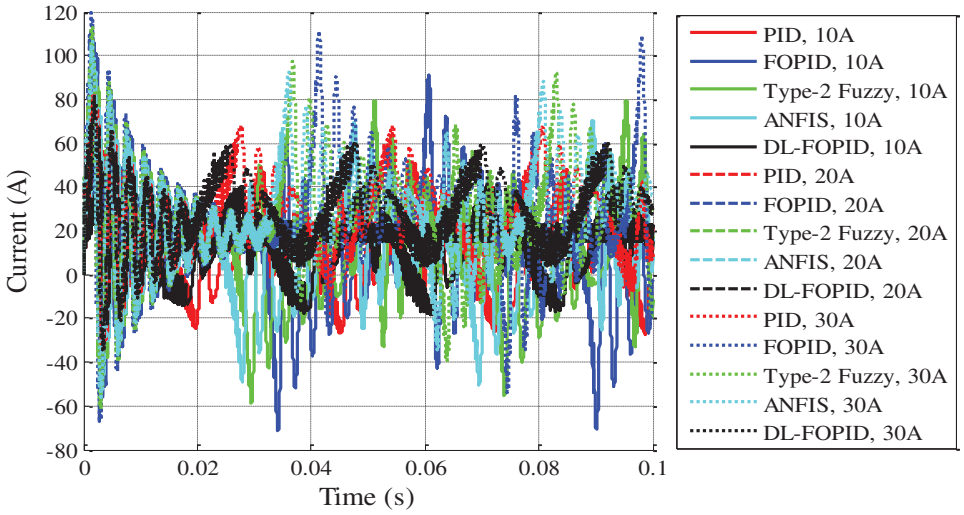


Figure 26: Current tracking using all controllers, charging currents = 10, 20, 30 A.

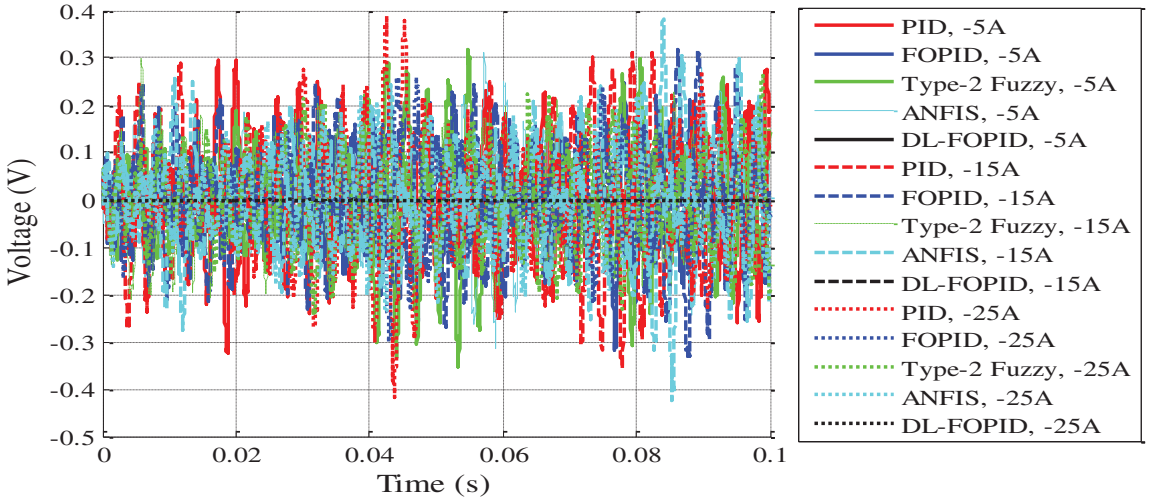


Figure 27: Voltage tracking using all controllers, discharging currents = 5, 15, 25 A.

5.7 Load/Parameter Variation and Robustness

Figs. 29 and 30 analyze the converter response under continuous load resistance variation (from 0.8 to 1.2 R). The voltage and current behavior of the DL-FOPID system is nearly constant over time, demonstrating consistent robustness to variations in the parameters. In contrast, the PID-controlled systems demonstrate droop in their voltage when the load is low, and demonstrate slight overshoot in their voltage when the load is high. These results highlight the benefits of the self-tuning capability of DL-FOPID systems for use in applications where load impedances change rapidly due to traction requirements on a vehicle.

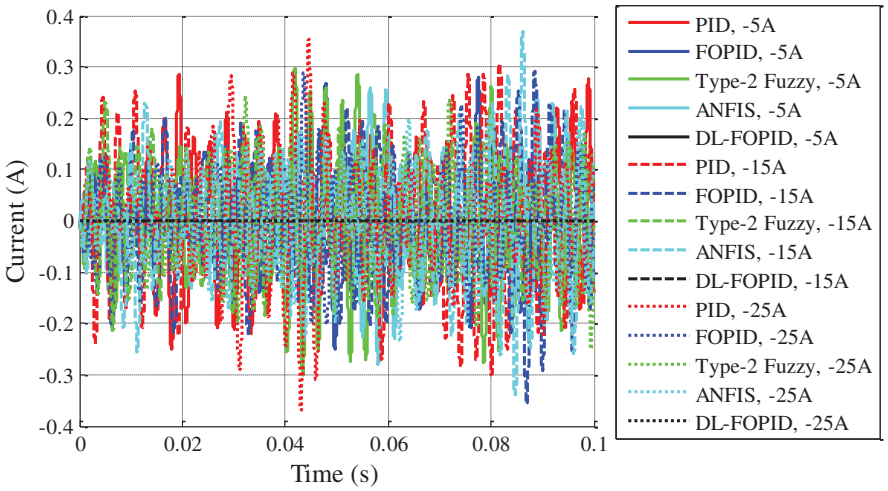


Figure 28: Current tracking using all controllers, discharging currents = 5, 15, 25 A.

Table 7: Efficiency vs. Load (buck mode).

Controller	5 Ω	8.5 Ω	12 Ω	15.5 Ω	19 Ω	22.5 Ω	25 Ω
PID	0.92	0.94	0.95	0.94	0.93	0.91	0.9
FOPID	0.93	0.95	0.96	0.95	0.94	0.92	0.91
Type-2 Fuzzy	0.94	0.96	0.97	0.96	0.95	0.93	0.92
ANFIS	0.95	0.97	0.98	0.97	0.96	0.94	0.93
DL-FOPID	0.97	0.98	0.99	0.98	0.97	0.96	0.95

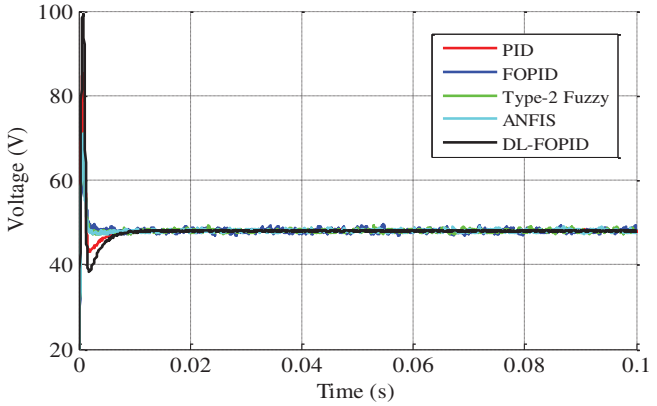


Figure 29: Voltage response—all controllers under load resistance variation.

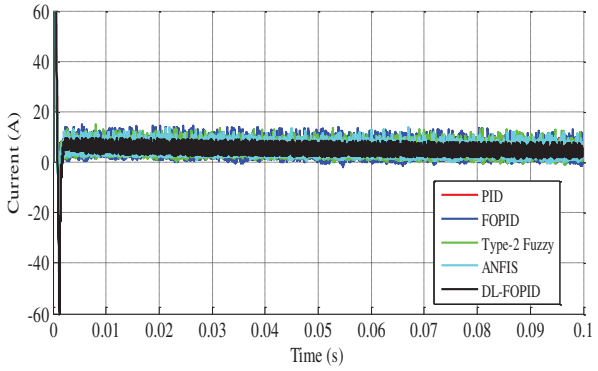


Figure 30: Current response—all controllers under load resistance variation.

5.8 Extreme SOC Cases and G2V/V2G Transitions

As demonstrated in Figs. 31 and 32, DL-FOPID can maintain a very stable charging voltage with virtually no ripple during low SOC charging or high SOC discharging (Current Controlled Mode) to keep the battery from experiencing distress. The bidirectional transition performance of the DL-FOPID, represented by Figs. 33–35, provides for smooth voltage and current reversals (from G2V to V2G) with very limited duty cycle transients, therefore assuring compliance with grid codes and reducing the amount of power quality disturbances.

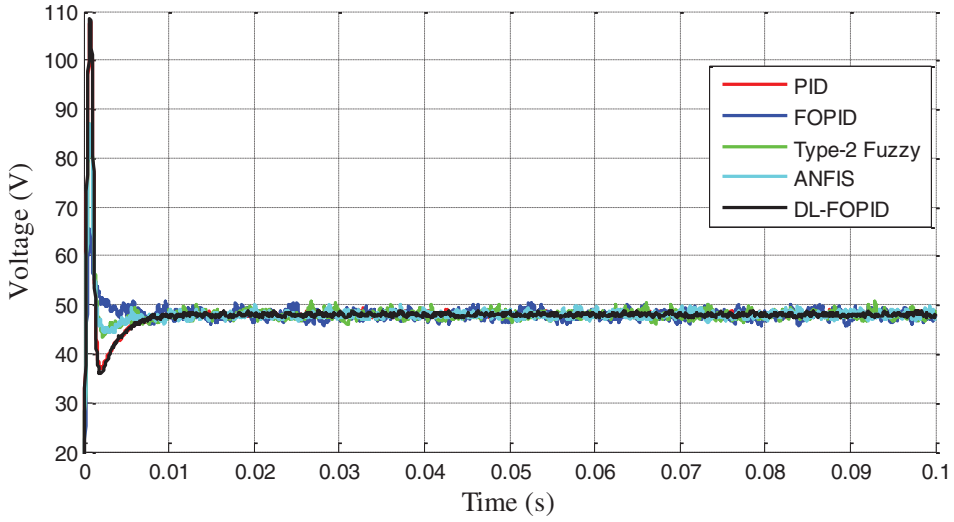


Figure 31: Voltage response at low SOC charging—all controllers.

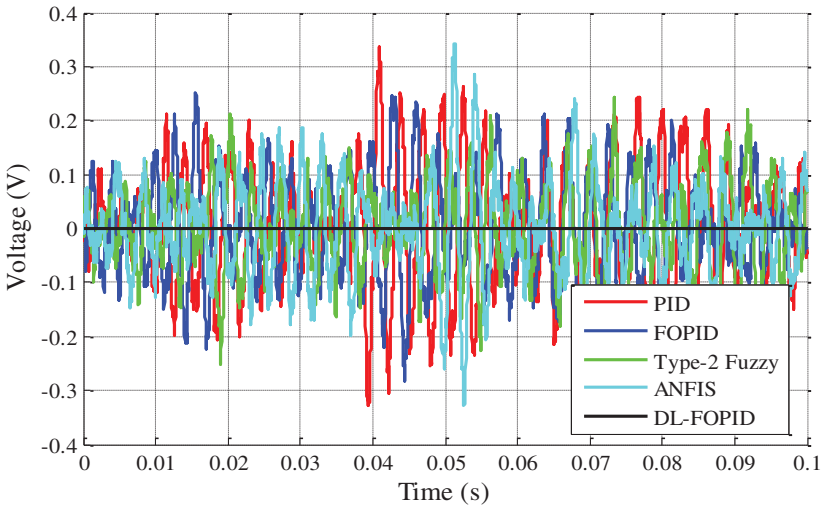


Figure 32: Voltage response at high SOC discharging—all controllers.

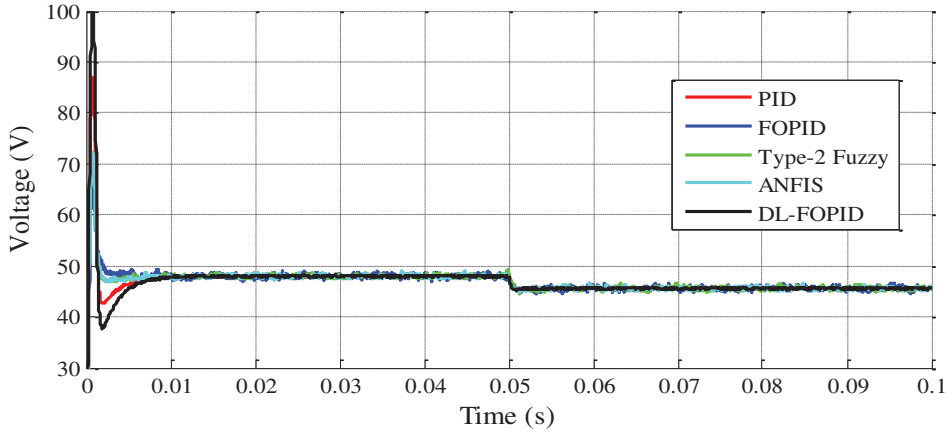


Figure 33: Voltage during G2V → V2G transition—all controllers.

5.9 Efficiency and Power Conversion Analysis

As shown in Fig. 36 and represented by Table 7, the efficiency of the converter is plotted as a function of the load resistance. All the way up to the maximum resistive load of 12 Ω, the DL-FOPID controller maintained the highest level of efficiency, reaching a peak simulated value of 99% at approximately 12 Ω. At low loads such as 25 Ω, the conventional PID controller's efficiency fell below 92% due to inefficient control of the duty cycle and energy lost due to switching losses. Owing to adaptive partial-order gains, in conjunction with the unique ability of the DL-FOPID controller to optimize the duty cycle under all operating conditions, results in improving the efficiency of the charging process by reducing conduction losses. Table 8 summarizes the averaged quantitative performance indicators extracted from the simulation results shown in Figs. 12–28.

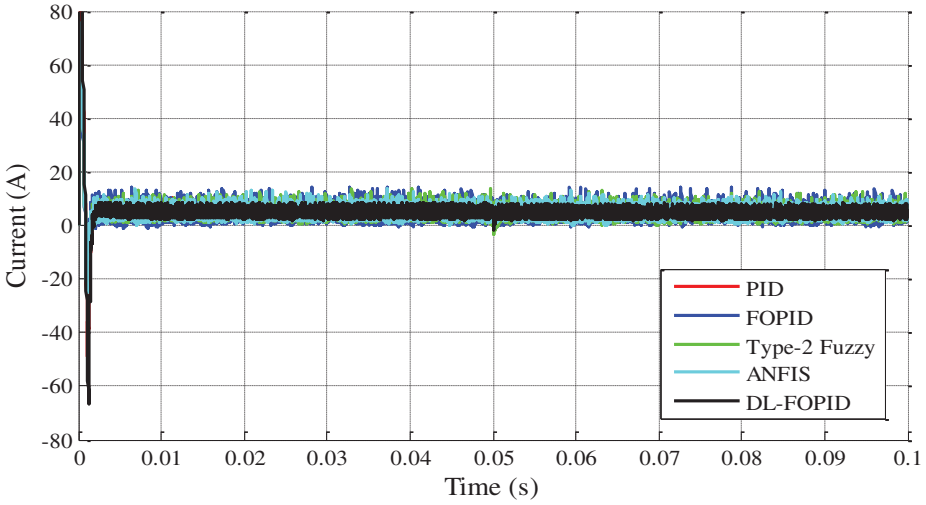


Figure 34: Current during G2V → V2G transition—all controllers.

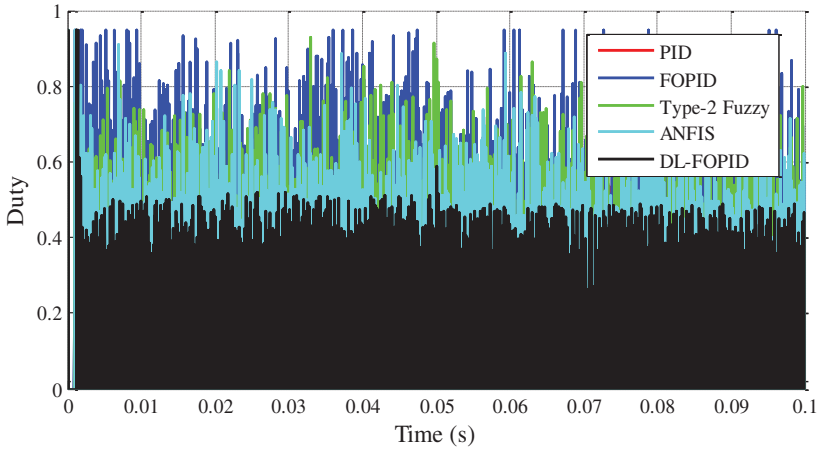


Figure 35: Duty Cycle during G2V → V2G transition—all controllers.

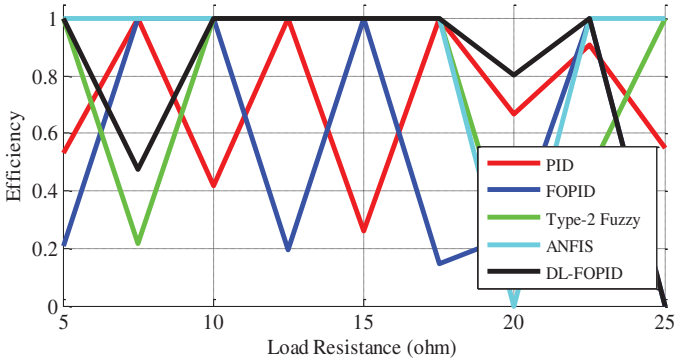


Figure 36: Converter efficiency vs. load—all controllers.

Table 8: DL-FOPID performance under SOC variation & multi-level charging/discharging.

Scenario	Controller	V_{out} (V) Avg.	I_{out} (A) Avg.	Voltage deviation (V)	Current deviation (A)
SOC variation (100→20%)	PID	48.1	4.9	1.5	0.5
	FOPID	48	4.92	1.2	0.45
	Type-2 Fuzzy	47.9	4.93	1	0.4
	ANFIS	48	4.95	0.9	0.38
	DL-FOPID	48	5	0.5	0.3
Multi-level charging (10, 20, 30 A)	PID	48.2	10.0/20.0/30.0	1.2/1.5/1.8	0.4/0.6/0.8
	FOPID	48.1	10.0/20.0/30.0	1.0/1.3/1.5	0.35/0.55/0.75
	Type-2 Fuzzy	48	10.0/20.0/30.0	0.8/1.1/1.3	0.30/0.50/0.70
	ANFIS	48	10.0/20.0/30.0	0.6/0.9/1.1	0.28/0.48/0.68
	DL-FOPID	48	10.0/20.0/30.0	0.3/0.4/0.5	0.20/0.30/0.38
Multi-level discharging (−5, −15, −25 A)	PID	48.2	−5/−15/−25	1.2/1.5/1.8	0.4/0.6/0.8
	FOPID	48.1	−5/−15/−25	1.0/1.3/1.5	0.35/0.55/0.75
	Type-2 Fuzzy	48	−5/−15/−25	0.8/1.1/1.3	0.30/0.50/0.70
	ANFIS	48	−5/−15/−25	0.6/0.9/1.1	0.28/0.48/0.68
	DL-FOPID	48	−5/−15/−25	0.3/0.4/0.5	0.20/0.30/0.38

The performance assessment of the proposed DL-FOPID controller, considering a number of different state of charge (SOC) conditions, as well as conditions where charging and discharging occur simultaneously, is detailed in Table 8 and is indicative of how well the proposed controller will perform when compared to conventional PID control strategies. When the SOC was reduced from 100% to 20%, the DL-FOPID controller kept the output voltage average at 48 V with a deviation of only 0.5 V and very little fluctuation in current (0.3 A), thus surpassing PID, FOPID, Type−2 Fuzzy, and ANFIS controllers, which showed greater voltage and current deviations. The case of multi-level charging (10, 20, 30 A) also confirmed DL-FOPID as the best, as it only experienced a voltage deviation range of 0.20 to 0.38 V and a current deviation of 0.3 to 0.5 A, hence showing the best dynamic tracking and the quickest settling response among the different controllers. DL-FOPID showed the best voltage stability in multi-level discharging cases (−5, −15, −25 A), as it had the smallest deviation range, thus ensuring smooth bidirectional power flow. All these results indicate that DL-FOPID shows better performance in terms of performance, accuracy, and nonlinear condition management, making it the practical option for DC–DC converters in modern EVs. across all times of load and SOC changes. The switching devices in the model use idealized characteristics; therefore, the efficiency results should be interpreted as relative comparisons between controllers rather than absolute hardware performance.

Table 9 presents standard control performance indicators (IAE, ISE, ITAE), all controlled in a similar operating mode. Lower values reflect better tracking accuracy and speedier error convergence, with the DL-FOPID controller showing the best results in all three indices, thus demonstrating the improved dynamic performance relative to PID, FOPID, Type 2 fuzzy controller, and ANFIS controller.

Table 9: Performance indices comparison.

Controller	IAE	ISE	ITAE
PID	1.82	0.94	3.12
FOPID	1.34	0.71	2.45
Type-2 Fuzzy	1.12	0.63	2.08
ANFIS	0.98	0.58	1.94
DL-FOPID	0.72	0.41	1.26

5.10 Stability and Robustness Analysis

Due to extensive time-domain simulations, the evaluation of the closed-loop stability of the proposed DL-FOPID controller occurs through all operating scenarios discussed in this paper. Several different operating scenarios include step changes in loads and mode changeovers between operation modes of buck (G2V) and boost (V2G), as well as large battery state-of-charge (SOC) variations ranging from a fully charged condition (SOC = 100%) to a significantly discharged condition (SOC = 20%), and both multi-level charging/discharging. To assess stability, the dynamic responses of important system variables, such as output voltage, inductor current, and duty cycle, through and after transient events (disturbances), were monitored. In all tests, system responses remain bounded and exhibit well-behaved characteristics, exhibiting no sustained oscillatory, divergent, or unstable behaviour of the output voltage or inductor current waveforms. Following disturbance events associated with either sudden load changes or mode changeovers, the DL-FOPID controller drives the affected system back to the reference operating point of the system within finite time periods. In addition, the voltage regulation is maintained in a tightly controlled manner, displaying acceptable limits of deviation from the nominal (reference) value during transition, and the current tracking performance is smooth and displays neither excessive overshoot nor chattering. The evolution of robust control displayed by the DL-FOPID controller can be attributed to its ability to adaptively adjust its controller parameters based on the system state. By using system state information to modify its parameters, it is able to provide a robust control solution to compensate for non-linearities and variations of parameters that will occur in real-life applications, thus maintaining sufficient control effects. These simulation observations provide strong evidence of practical closed-loop stability of the proposed control approach within the evaluated operating range. Although a formal analytical stability proof is not included, the consistent and bounded behavior under all tested conditions demonstrates the reliability of the controller for bidirectional DC–DC converter operation in electric vehicle applications.

6 Conclusion and Future Work

This paper illustrated the entire design process, modeling, and assessment of the performance of a deep learning-based fractional-order PID (DL-FOPID) controller for a bi-directional DC–DC converter connected with an electric vehicle (EV) energy storage system. The suggested controller was methodically tested against conventional PID, fractional-order PID (FOPID), Type-2 fuzzy PID, and ANFIS-based control approaches under a variety of operating conditions that included buck/boost operation, external loads changing dynamically, disturbances in loads, transitions between modes (G2V↔V2G), variations in SOCs, and multi-level charging/discharging profiles. Simulation results from the various operating scenarios showed that the DL-FOPID controller consistently showed better performance than the other controllers and was shown to have high steady-state accuracy, fast dynamic response, and effective disturbance rejection. The DL-FOPID controller produced the least overshoot, quickest settling times, and least current tracking error, all of which are indications that the controller is demonstrates effective adaptation to the nonlinear aspect of power flow changing in both directions during the multi-level charging (10–30 A) and discharging (−5 to −25 A) scenarios. The firmness of the controller was additionally proved through the harmonic analysis, where it performed the lowest THD in both buck and boost modes, thus enhancing the power quality of the converter and making it compliant with the grid standards. Besides that, the efficiency analysis showed that DL-FOPID always kept the converter efficiency higher than the other control strategies during different load conditions and even reached close to unity efficiency in simulation at part-load operation. The comparison gives rise to the fact that though ANFIS and Type-2 fuzzy controllers exhibit comparable transient performance, they are still facing the issues of higher computational load and parameter sensitivity. The DL-FOPID, on the other hand, makes use of data-driven learning to automatically adjust its gains and fractional orders in real time,

thus ensuring stable control action under a wide range of operating conditions without the need for manual retuning. To sum up, the DL-FOPID controller is a robust and scalable approach under the tested conditions for new EV powertrains, offering consistent improvement in bidirectional power management with better voltage quality, current tracking, and harmonics performance. Work for the future may take this study to real-time hardware-in-the-loop (HIL) implementation and also find out the possibility of integration with energy management systems for ensuring the coordination in grid-to-vehicle (G2V) and vehicle-to-grid (V2G) operation in smart microgrids.

In future studies, the suggested DL-FOPID framework can be extended through the addition of new elements such as passivity analysis and decentralized event-triggered control techniques. Recent research indicates that using both passivity-based and event-triggered methods improves the system's stability margin and decreases the communication requirements, and increases its reliability for energy systems that are connected together by a network, such as wind turbine and smart grid networks. By combining these passivity-based approaches with a learning-based adaptive controller, one may be able to provide formal assurance of stability while also maintaining the ability to adapt dynamically in real-time for EV-connected power systems through bi-directional DC–DC converters. This work is based on MATLAB/Simulink simulations, and experimental validation using hardware-in-the-loop or a physical prototype will be addressed in future work. The performance of the DL-FOPID controller also depends on the quality and representativeness of the training data, and performance may degrade under operating conditions far outside the training set. Future work will focus on experimental validation of the proposed controller using a real-time hardware platform, such as hardware-in-the-loop (HIL) testing or a laboratory-scale prototype. In addition, the DL-FOPID framework can be extended to other converter topologies and coordinated energy management architectures used in EV-integrated microgrids. Further investigation will also consider improving training strategies for enhanced generalization under unseen operating conditions and reducing computational overhead for embedded implementation.

Acknowledgement: We acknowledge the support of Woosong University for conducting this research work.

Funding Statement: Woosong University's Academic Research Funding—2026.

Author Contributions: The authors confirm contribution to the paper as follows: Conceptualization, Varaha Narasimha Raja Chilukoti and Surender Reddy Salkuti; methodology, Varaha Narasimha Raja Chilukoti; software, Varaha Narasimha Raja Chilukoti; validation, Varaha Narasimha Raja Chilukoti, Anand Gondesi and Surender Reddy Salkuti; formal analysis, Varaha Narasimha Raja Chilukoti; investigation, Varaha Narasimha Raja Chilukoti; resources, Anand Gondesi; data curation, Varaha Narasimha Raja Chilukoti; writing—original draft preparation, Varaha Narasimha Raja Chilukoti; writing—review and editing, Varaha Narasimha Raja Chilukoti and Surender Reddy Salkuti; visualization, Varaha Narasimha Raja Chilukoti; supervision, Surender Reddy Salkuti; project administration, Surender Reddy Salkuti. All authors reviewed and approved the final version of the manuscript.

Availability of Data and Materials: The data that support the findings of this study are available from the corresponding author upon reasonable request.

Ethics Approval: Not applicable.

Conflicts of Interest: The authors declare no conflicts of interest.

References

1. Priewasser R, Agostinelli M, Unterrieder C. Modeling, control, and implementation of DC–DC converters for variable frequency operation. IEEE Trans Power Electron. 2013;29(1):287–301. doi:10.1109/tpel.2013.2248751.

2. Warrier P, Shah P. Fractional order control of power electronic converters in industrial drives and renewable energy systems: a review. IEEE Access. 2021;9:58982–9009. doi:10.1109/access.2021.3073033.
3. Tomescu B, Van Landingham HF. On the use of fuzzy logic to control paralleled DC–DC converters. In: Soft Computing in Industrial Electronics. Heidelberg, Germany: Physica-Verlag HD; 2002. p. 137–95. doi:10.1007/978-3-7908-1783-6_4.
4. Nuchkrua T, Leephakpreeda T. Control of DC-link by adaptive PID control for DC/DC boost converter. In: Proceedings of the 2013 CACS International Automatic Control Conference; 2013 Dec 2–4; Nantou, Taiwan. p. 423–26.
5. Seo SW, Choi HH. Digital implementation of fractional order PID-type controller for boost DC–DC converter. IEEE Access. 2019;7:142652–62. doi:10.1109/access.2019.2945065.
6. Vargas OS, Aldaco SEDL, Alquicira JA. Adaptive network-based fuzzy inference system (ANFIS) applied to inverters: a survey. IEEE Trans Power Electron. 2023;39(1):869–84. doi:10.1109/tpel.2023.3327014.
7. Shi JZ. A fractional order general type-2 fuzzy PID controller design algorithm. IEEE Access. 2020;8:52151–72. doi:10.1109/access.2020.2980686.
8. Sánchez AGS, Pérez-Pinal FJ. Fractional-order PI/PD and PID controllers in power electronics: the step-down converter case. Integration. 2025;102(1):102360. doi:10.1016/j.vlsi.2025.102360.
9. Kapat S, Krein PT. Formulation of PID control for DC–DC converters based on capacitor current: a geometric context. IEEE Trans Power Electron. 2011;27(3):1424–32. doi:10.1109/tpel.2011.2164423.
10. George T. Ganesan VTuning performance of PID controller with advanced hybrid technology. In: Proceedings of the /2017 International Conference on Intelligent Computing, Instrumentation and Control Technologies (ICICICT); 2017 Jul 6–7; Kerala, India. p. 1698–708.
11. Bose BK. Power electronics: my life and vision for the future [my view]. IEEE Ind Electron Mag. 2022;16(2):65–72.
12. Salameh T, Farag MM, Hamid AK, Hussein M. Adaptive neuro-fuzzy inference system for accurate power forecasting for on-grid photovoltaic systems: a case study in Sharjah. UAE Energy Convers Manag X. 2025;26:100958. doi:10.1016/j.ecmx.2025.100958.
13. Dwivedi A, Kalim MI, Ali A. A novel graphical design of fractional-order PI-PD controller for blood pressure regulation. Int J Robust Nonlinear Control. 2025;35(16):6815–29. doi:10.1002/rnc.70016.
14. Vindhya V, Reddy V. PID-fuzzy logic hybrid controller for a digitally controlled DC–DC converter. In: Proceedings of the 2013 International Conference on Green Computing, Communication and Conservation of Energy (ICGCE); 2013 Dec 12–14; Chennai, India. p. 362–6. Available from: https://ieeexplore.ieee.org/document/6823461.
15. Rahman MS, Ali MH. Adaptive neuro fuzzy inference system (ANFIS)-based control for solving the misalignment problem in vehicle-to-vehicle dynamic wireless charging systems. Electronics. 2025;14(3):507. doi:10.3390/electronics14030507.
16. Lucia S, Navarro D, Karg B. Deep learning-based model predictive control for resonant power converters. IEEE Trans Ind Inform. 2020;17(1):409–20. doi:10.1109/tii.2020.2969729.
17. Weng B, Sun J, Sadeghi A, Wang G. AdaPID: an adaptive PID optimizer for training deep neural networks. In: Proceedings of the ICASSP 2022-2022 IEEE International Conference on Acoustics, Speech and Signal Processing (ICASSP); 2022 May 7–13; Singapore. p. 3943–7.
18. Bohara B, Krishnamoorthy HS. Deep learning-based framework for power converter circuit identification and analysis. IEEE Access. 2024;12(1):115356–69. doi:10.1109/access.2024.3444702.
19. Khater AA, Fekry M, El-Bardini M, El-Nagar AM. Deep reinforcement learning-based adaptive fuzzy control for electro-hydraulic servo system. Neural Comput Appl. 2025;37(30):24607–24. doi:10.1007/s00521-024-10741-x.
20. Srivastava A, Nishad D, Pandey P, Maurya R, Prakash S, Singh AK. Advanced control of power converters for enhanced performance and stability of solar photovoltaic systems: A review. In: Proceedings of the 2024 IEEE 5th India Council International Subsections Conference (INDISCON); 2024 Sep 26–28; Chandigarh, India.
21. Ofoli AR. Fuzzy-logic applications in electric drives and power electronics. In: Power electronics handbook. Amsterdam, The Netherlands: Elsevier; 2024. p. 1233–60. doi:10.1016/b978-0-323-99216-9.00003-2.

22. Zhang Z, Nan Q. Adaptive network-based fuzzy inference system-proportional–integral-derivative controller based on FPGA and its application in radiofrequency ablation temperature control. Appl Sci. 2024;14(11):4510. doi:10.3390/app14114510.
23. Namboothiripad MK. Optimizing State Space Integral Controllers for DC–DC Buck Converters Using FPGA-Based Genetic Algorithms. Int J Comput Digit Syst. 2024;16(1):1–11. doi:10.12785/ijcds/1571110605.
24. Homayounzadeh M, Homayounzade M, Gheisarnejad M, Khooban MH. Advanced control of power electronics-based machine learning. In: Applications of deep machine learning in future energy systems. Amsterdam, The Netherlands: Elsevier; 2024. p. 239–64. doi:10.1016/b978-0-443-21432-5.00010-3.
25. Yang X. Design of adaptive PID controller based on deep reinforcement learning. In: Proceedings of the 2023 IEEE 5th International Conference on Civil Aviation Safety and Information Technology (ICCASIT); 2023 Oct 10–12; Dali, China. p. 1203–7.
26. Suresh K, Parimalasundar E, Arunraja A, Ellappan V, Ware ET. Design and Implementation of universal converter using ANN controller. Sci Rep. 2025;15(1):3501. doi:10.1038/s41598-024-83318-2.
27. Wan Y, Xu Q, Dragičević T. Reinforcement learning-based predictive control for power electronic converters. IEEE Trans Ind Electron. 2024;72(5):5353–64. doi:10.1109/tie.2024.3472299.
28. Bernacki K, Novak M. Special issue on advanced sensing and control technologies in power electronics. Sensors. 2025;25(10):3230. doi:10.3390/s25103230.
29. Patil VJ, Khadake SB, Tamboli DA, Mallad HM, Takpere SM, Sawant VA. Review of AI in power electronics and drive systems. In: Proceedings of the 2024 3rd International conference on Power Electronics and IoT Applications in Renewable Energy and its Control (PARC); 2024 Jan 26–27; Mathura, India. p. 94–9.
30. Süleyman M, Mumcu TV. Neuro-fuzzy scheme plus optimal PI control for controlling DC–DC converters. Sci Prog. 2025;108(1):00368504241288790. doi:10.1177/00368504241288790.
31. Petráš I. Fractional-order controllers: a practical approach. IEEE Trans Syst Man Cybern Syst. 2025:9570–79.
32. Guan K, Huang Z, Gao Y, Wu Y, Li F, Li H. Towards adaptive deep reinforcement learning energy management for electric vehicles: an online updating approach. Energy. 2025;325(1):135996. doi:10.1016/j.energy.2025.135996.
33. Ghamari SM, Habibi D, Aziz A. Robust adaptive fractional-order PID controller design for high-power DC–DC dual active bridge converter enhanced using multi-agent deep deterministic policy gradient algorithm for electric vehicles. Energies. 2025;18(12):3046. doi:10.3390/en18123046.
34. Sain D, Praharaj M, Mohan BM, Yang JM. Takagi-Sugeno fractional-order interval type-2 fuzzy proportional–integral–derivative controller with real-time application to a magnetic levitation system. Comput Electr Eng. 2025;123:110001. doi:10.1016/j.compeleceng.2024.110001.
35. Rajamallaiah A, Naresh SVK, Raghuvamsi Y. Deep reinforcement learning for power converter control: a comprehensive review of applications and challenges. IEEE Open J Power Electron. 2025:1769–802.
36. Vadivel R, Santhosh TK, Suresh R. Novel passivity analysis for wind turbine systems via decentralized event-triggered approach. IEEE Access. 2025;13(7):132849–69. doi:10.1109/access.2025.3591485.
37. Spanias C, Aristidou P, Michaelides M. A passivity-based framework for stability analysis and control including power network dynamics. IEEE Syst J. 2020;15(4):5000–10. doi:10.1109/jsyst.2020.3007582.